

¹ Chapter 1

² Charge monitoring – the ATLAS ³ Diamond Beam Monitor

⁴ Particle detectors in high energy physics experiments need to meet very stringent
⁵ specifications, depending on the functionality and their position in the experiment.
⁶ In particular, the detectors close to the collision point are subject to high levels of
⁷ radiation. Then, they need to operate with a high spatial and temporal segmentation
⁸ to be able to precisely measure trajectories of hundreds of particles in very short time.
⁹ In addition, they need to be highly efficient. In terms of the structure, their active
¹⁰ sensing area has to be thin so as not to cause the particles to scatter or get stopped,
¹¹ which would worsen the measurements. This also means that they have to have a low
¹² heat dissipation so that the cooling system dimensions can be minimised. Finally,
¹³ they need to be able to operate stably for several years without an intervention,
¹⁴ because they are buried deep under tonnes of material and electronics.

¹⁵ The material of choice for the inner detector layers in the HEP experiments is
¹⁶ silicon. It can withstand relatively high doses of radiation, it is highly efficient (of the
¹⁷ order of $\sim 99.9\%$) and relatively low cost due to using existing industrial processes
¹⁸ for its production. Its downside is that, with increasing irradiation levels, it needs to
¹⁹ be cooled to increasingly low temperatures to still operate stably.

²⁰ The ATLAS Diamond Beam Monitor (DBM) is a novel high energy charged par-
²¹ ticle detector. Its function is to measure luminosity and beam background in the
²² ATLAS experiment. The monitor's pCVD diamond sensors are instrumented with
²³ pixellated FE-I4 front-end chips. The pCVD diamond sensor material was chosen
²⁴ to ensure the durability of the sensors in a radiation-hard environment. The DBM
²⁵ was designed as an upgrade to the existing luminosity monitor called the Beam Con-
²⁶ ditions Monitor (BCM) [] consisting of eight diamond pad detectors, which is able
²⁷ to perform precise time-of-flight (ToF) measurements. The DBM complements the
²⁸ BCM's features by implementing tracking capability. Its pixelated front-end elec-
²⁹ tronics significantly increase the spatial resolution of the system. Furthermore, the
³⁰ DBM is able to distinguish particle tracks originating in the collision region from the
³¹ background hits. This capability is a result of its projective geometry pointing to-
³² wards the interaction region. This chapter first describes the principles of luminosity

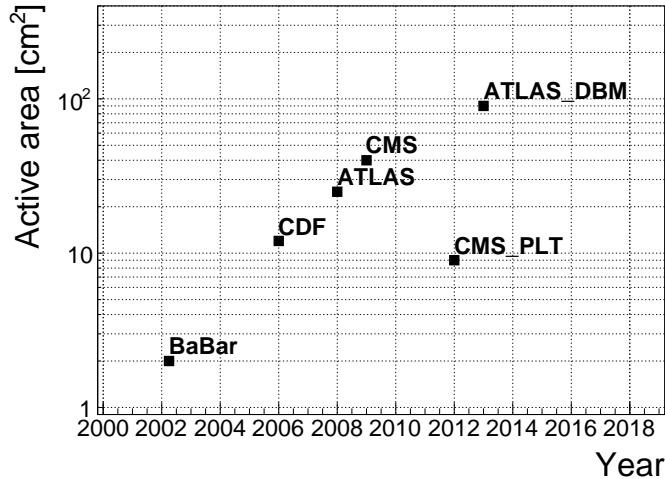


Figure 1.1: Diamond detectors installed in high-energy physics experiments in the last decade, sorted by the active sensor area. The first four detectors from the left are radiation monitors whereas the right two are pixel trackers.

33 measurements. It then explains how the DBM will carry out this task. Finally, some
 34 results from tests and from the real collisions are presented.

35 When a particle traverses a sensor plane, a hit is recorded in the corresponding
 36 pixel. Thus, a precise spatial and timing information of the hit is extracted. With
 37 three or more sensors stacked one behind the other, it is also possible to define the
 38 particle’s trajectory. This is the case with the DBM. Its projective geometry allows
 39 the particles to be tracked if they traverse the sensor planes. The DBM relates the
 40 luminosity to the number of particle tracks that originate from the collision region
 41 of the ATLAS experiment. Particles that hit the DBM from other directions are not
 42 taken into account.

43 The DBM is not the first diamond detector used in HEP, but it is the largest
 44 pixellated detector installed so far (see figure 1.1).

45 1.1 Luminosity measurements

46 Luminosity is one of the most important parameters of a particle collider. It is
 47 a measurement of the rate of particle collisions that are produced by two particle
 48 beams. It can be described as a function of beam parameters, such as: the number of
 49 colliding bunch pairs, the revolution frequency, the number of particles in each bunch
 50 and the transverse bunch dimensions. The first four parameters are well defined.
 51 However, the transverse bunch dimensions have to be determined experimentally
 52 during calibration. The ATLAS experiment uses the *van der Meer scan* [] during
 53 low-luminosity runs to calibrate the luminosity detectors. This scan is performed
 54 by displacing one beam in a given direction and measuring the rate of interactions
 55 as a function of the displacement. Transverse charge density of the bunches can be

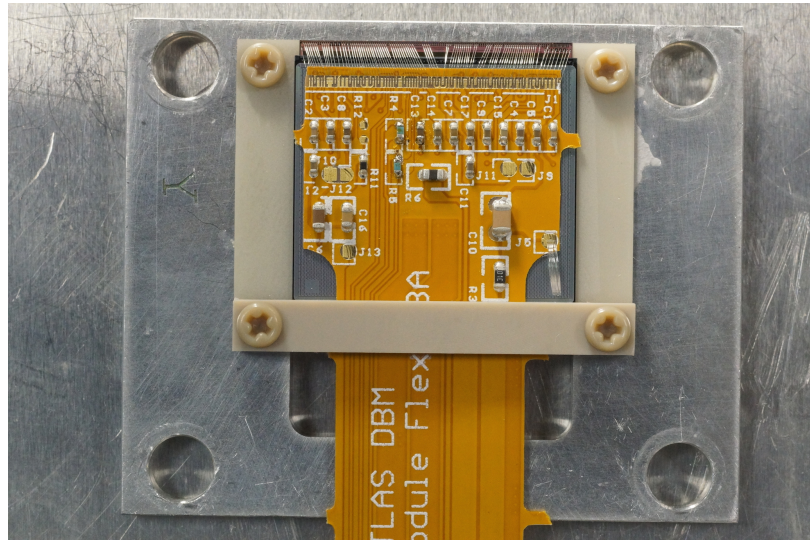


Figure 1.2: DBM module, top-down view. Visible is the flexible PCB with signal and power connections, the silicon sensor and a part of the FE-I4. Wire bonds from the PCB to the FE-I4 and to the sensor are also visible.

56 estimated on the basis of the interaction rate. The calibrated luminosity detectors
57 can then operate during high-luminosity runs.

58 One approach to luminosity monitoring is to count the number of particles pro-
59 duced by the collisions. The luminosity is then proportional to the number of detected
60 particles. A detector has to be capable of distinguishing individual particles that fly
61 from the interaction point through the active sensor area. If the detector has at least
62 three layers, it can reconstruct the particle’s track, which gives us more information
63 on the particle’s trajectory. This is one reason why detectors with a high time and/or
64 spatial segmentation are more suitable for these applications. The second reason is
65 that, with a high spatial segmentation, the detector will not saturate even at high
66 particle fluencies.

67 1.2 Diamond pixel module

68 The two most important parts of the diamond pixel module (seen in figure 1.2) are
69 the sensor, which detects ionising radiation, and the pixellated front-end chip, which
70 collects the ionised charge, processes the recorded data and sends it to the readout
71 system. This section describes the two main parts and their interconnection.

72 1.2.1 Sensors

73 The DBM modules are equipped with two types of sensors – diamond and silicon.
74 The silicon sensors are used as a fallback solution because there were simply not
75 enough high-quality diamond sensors available. In addition, a comparative study of
76 irradiation damage between silicon and diamond can be made.

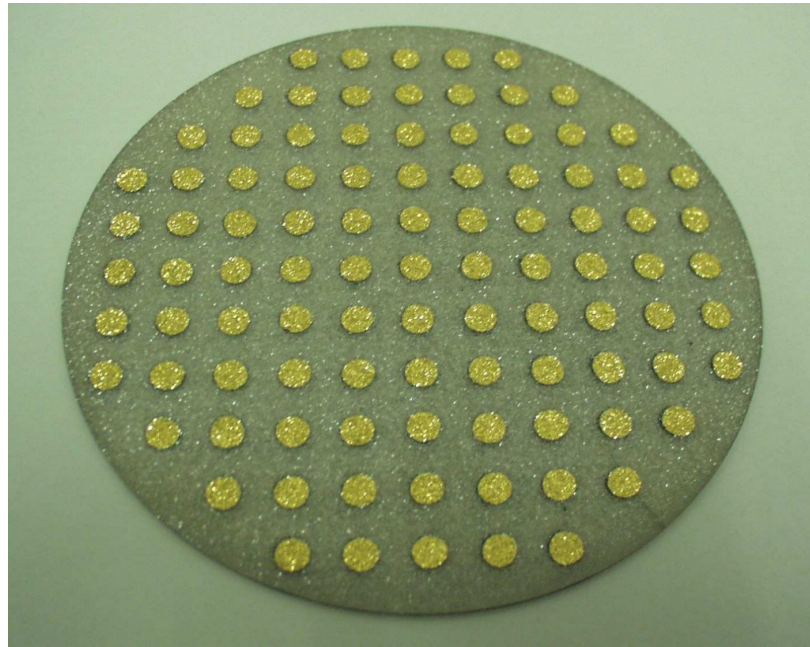


Figure 1.3: A pCVD wafer. Golden dots on the surface are the electrodes that were applied to test the wafer across the surface and find the regions with the highest efficiency.

77 **Diamond sensors** The target material for this application is pVCD diamond, because the active area of an individual sensor must be approximately 4 cm^2 , which is 78 too large for the sCVD diamond. pCVD is also a bit cheaper, which makes a detector 79 with a large active area more feasible to build. The samples were provided by three 80 companies: DDL, E6 and II-IV. They are grown in 15 cm wafers, as seen in figure 1.3. 81 Their thickness is equal to 500 μm and the minimum required charge collection efficiency 82 is 40 %. They need to operate at bias voltages between 600–1000 V. On one 83 side there is a single gold electrode whereas on the other side a pixellised metallisation 84 is placed.

85 **Silicon sensors** were taken from the IBL production. They are standard $n^+ - in - n$ planar sensors with a 200 μm thickness and were fabricated at CiS, a German 86 company. They are designed to have nearly a 100 % efficiency when non-irradiated. 87 Their bulk resistivity is between 2–5 $\text{k}\Omega\text{cm}$ and they were diffusion oxygenated at 88 1150 °C for 24 hours to increase their radiation hardness. One side is segmented into 89 pixels. Guard rings at the edges of the sensor provide a controlled drop in potential, 90 reducing the possibility of shorts at maximum design bias voltages of the order of 91 1000 V.

94 1.2.2 Front-end electronics

95 The FE-I4 (front-end version four) is an ASIC pixel chip designed specifically for the 96 ATLAS pixel detector upgrade. It is built as a successor to the current pixel chip

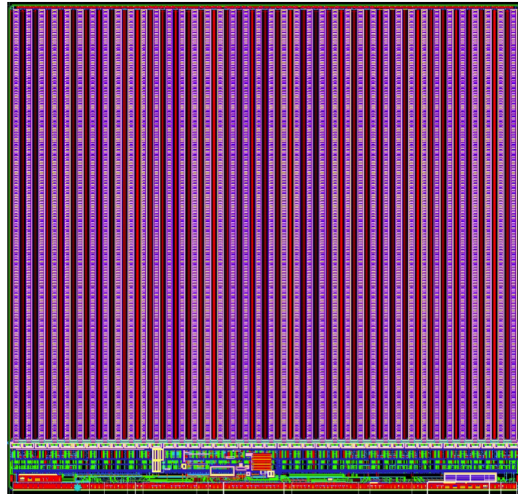


Figure 1.4: FE-I4 layout, top-down view. The pink area are pixels grouped into columns, the green area below is the common logic and the red strip at the bottom are the wire bond pads.

97 FE-I3, surpassing it in size of the active area ($4\times$ larger) as well as the number of
 98 channels/pixels ($10\times$ more). 336 such FE-I4 modules are used in the newly installed
 99 pixel layer called the Insertable B-Layer (IBL) [], as well as the DBM. The FE-I4's
 100 integrated circuit contains readout circuitry for 26880 pixels arranged in 80 columns
 101 on a $250\text{ }\mu\text{m}$ pitch and 336 rows on a $50\text{ }\mu\text{m}$ pitch. The size of the active area is
 102 therefore $20.0 \times 16.8\text{ mm}^2$. This fine granularity allows for a high-precision particle
 103 tracking. The chip operates at 40 MHz with a 25 ns acquisition window, which corre-
 104 sponds to the spacing of the particle bunches in the LHC. It is hence able to correlate
 105 hits/tracks to their corresponding bunch. Furthermore, each pixel is capable of mea-
 106 suring the deposited charge of a detected particle by using the Time-over-Threshold
 107 (ToT) method. Finally, the FEI4 has been designed to withstand a radiation dose up
 108 to 300 MGy. This ensures a longterm stability in the radiation hard forward region
 109 of the ATLAS experiment.

110 Each pixel is designed as a separate entity. Its electrical chain is shown in fig-
 111 ure 1.5. The bump-bond pad – the connection to the outside of the chip – is the
 112 input of the electrical chain, connected to a free-running amplification stage with ad-
 113 justable shaping using a 4-bit register at the feedback branch. The analog amplifier is
 114 designed to collect negative charge, therefore electrons. The output is routed through
 115 a discriminator with an adjustable threshold. This value in effect defines the level at
 116 which the circuit will detect a hit. In addition, there is a counter of the clock cycles
 117 (25 ns sampling) during which the signal is above the discriminator threshold. The
 118 value of the counter is proportional to the collected charge. The logic gates at the end
 119 of the chain are used to enable/disable the pixel and to issue a so-called HitOr flag –
 120 this signal is set whenever at least one of the pixels was hit and is used as a trigger for
 121 the readout. The output of the chain – HitOut – is routed into the chip's logic where
 122 it is buffered and eventually sent out to the readout system. The module receives all

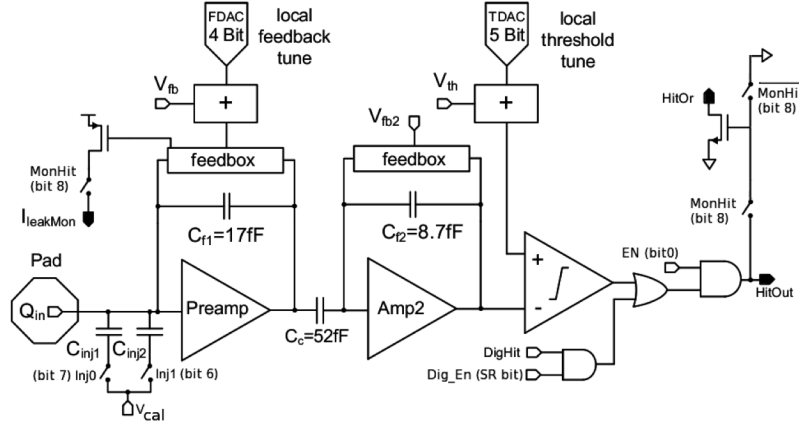


Figure 1.5: Schematic of an analog pixel. Courtesy of the FE-I4 collaboration.

123 its commands from the system via a 40 MHz LVDS line. The commands are either
 124 settings for the pixel registers or triggers that start the data readout. The data are
 125 sent via an LVDS line at up to 320 Mbit/s, but by default at 160 Mbit/s, four times
 126 faster than the device clock. This enables the device to clear out its buffers before
 127 new data are recorded, thus avoiding dead time. The FE-I4 has been successfully
 128 tested for trigger rates of up to 300 kHz.

129 The DBM uses pCVD diamond with $d_C = 500 \mu\text{m}$ thickness and silicon with
 130 $d_{Si} = 200 \mu\text{m}$ thickness as a sensor material. The resulting most probable value
 131 (MPV) of the deposited charge for a minimum ionising particle (MIP) is calculated
 132 with the formula $Q_S = d \cdot E_{e-h}$ and equals 18000 electrons and 17800 electrons,
 133 respectively, at a full charge collection efficiency. Unfortunately this is not the case
 134 with the pCVD material, whereby we can expect the charge collection efficiency to
 135 be of the order of 50 % – around 9000 e. These values further decrease with received
 136 irradiation dose. Therefore in order to detect the particles depositing energy on the
 137 far left side of the landau spectrum, the threshold has to be set to a significantly
 138 lower value. On the other hand, too low threshold means that the electronic noise
 139 will trigger a false hit. The typical noise amplitudes being in the range of 120–200 e,
 140 a safe threshold range would be between $Th = 1000\text{--}3000$ e.

141 The analog amplifier is implemented in two stages to get a fast rise time at a
 142 low noise and a low power consumption. The output signal of the analog amplifier
 143 has a triangular shape with a fast rise time and a long decay. The shape can be
 144 adjusted by tuning the amplifier feedback loop. Its length is proportional to the
 145 collected charge, but it needs to be calibrated first. This is done using the injection
 146 capacitors C_{inj1} and C_{inj2} seen in figure 1.5 with well defined capacitances. A charge
 147 $Q_{cal} = V_{cal} \cdot (C_{inj1} + C_{inj2})$ is injected into the analog chain, the length of the output
 148 pulse is measured and the feedback value is changed to either lengthen or shorten
 149 the pulse in order to get to the required duration t_{cal} . The typical values are $Q_{cal} =$
 150 $5000\text{--}16000$ e at the time $t_{cal} = 5\text{--}10$ ToT, depending on the sensor, radioactive
 151 source and application. Therefore the initial threshold Th at 1 ToT and the calibrated

152 value Q_{cal} at t_{cal} ToT give us a linear scale of collected charge with respect to time
 153 over threshold. However, in practice this relation is nonlinear for lower thresholds,
 154 but since the goal of the measurements is to track the particles rather than to measure
 155 their deposited energy precisely, this is sufficient.

156 1.3 Module assembly and quality control

157 Parts for the detector arrived separately and were assembled into modules at CERN’s
 158 DSF lab after being checked for production faults. The assembled modules underwent
 159 a series of quality control (QC) and burn-in tests to determine their quality, efficiency
 160 and long-term stability.

161 1.3.1 Assembly

162 A single-chip module consists of a pixel module, a flexible PCB and the supporting
 163 mechanics (a ceramic plate and an aluminium plate). The chip arrives already bump-
 164 bonded to the sensor, be it diamond or silicon. First it is glued to the ceramic plate
 165 on one side and to the PCB on the other using either Araldite 2011 or Staystik
 166 672/472. The choice of glue was a topic of a lengthy discussion. Staystik is re-
 167 workable and has a very high thermal conductivity. The latter is important because
 168 the FE-I4 chips tend to heat up significantly and need a good heat sink. The problem
 169 is that it has a curing temperature of 160/170 °C. This temperature could cause some
 170 unwanted tension build-up between the FE-I4 and the diamond sensor due to different
 171 coefficients of thermal expansion, disconnecting regions of pixels. To avoid this, an
 172 alternative glue was tried. Araldite 2011 can be cured at lower temperatures – down
 173 to RT – but it has a lower heat conductivity. In the end Araldite was chosen as the
 174 safer option. However, due to the longer curing, the whole assembly process using
 175 Araldite is extended to two working days. After curing, the module is wire-bonded
 176 and attached to the aluminium plate using screws made up of a radiation-resistant
 177 PEEK plastic. They have to be tightened with a great care, because their screw head
 178 is only 0.2–0.6 mm away from the sensor edge – the sensor displacement tolerance
 179 during gluing is of the order of 0.5 mm. Finally, the module is put in an aluminium
 180 carrier which protects the module from mechanical damage or electrostatic discharges.

181 1.3.2 Testing

182 The modules were tested in the lab using an RCE readout system and a moving stage
 183 with two degrees of freedom. They were placed onto the stage and connected to the
 184 readout system and the power supplies. After ensuring the low- and high voltage
 185 connectivity they were checked for the signal connectivity. If everything was opera-
 186 tional, a series of automated tests was run. Each of these tests calibrates a certain
 187 value within a pixel, whether it is the signal threshold or the value for integrated

charge. These are tuned in a way that the response to a predefined calibration signal is uniform for all pixels across the sensor. This procedure is referred to as *tuning*.

When the modules were tuned, they were tested using a ^{90}Sr radioactive source. Two things were tested: 1) operation of all pixels and 2) sensor efficiency. The first test was carried out by moving the module slowly under the source while taking data so that the whole surface was scanned uniformly. The resulting occupancy map revealed any pixels that were not electrically connected to the sensor via bump bonds. This was an important step in the DBM QC procedure, because it turned out that a significant portion of the flip-chipped diamond sensors exhibited very poor connectivity. The disconnected regions on the faulty modules ranged anywhere from 0.5–80 % of the overall active surface. In two cases the sensor was even completely detached from the chip. The pixel connectivity turned out to be the most important qualification factor in the QC procedure. Unfortunately the only way to check it was to fully assemble a module and test it using a radioactive source. If the module turned out to be of poor quality, it was disassembled and sent for rework. The turnover time of this operation was of the order of one month, which affected the detector installation schedule significantly. Only the sensors that passed the pixel connectivity test underwent the second test stage in which the sensor's efficiency was estimated. In principle, a scintillator placed underneath the module was used as a trigger; a particle that crossed the DBM module and hit the scintillator, triggered the module readout. In the end, the number of triggers was compared to the number of hits/clusters recorded by the module. The resulting ratio was an estimate of the sensor's detection efficiency. The real sensor efficiency can only be measured in a particle beam and using a beam telescope as a reference detector. Nonetheless, the so-called *pseudo-efficiency* gave a rough estimate of the sensors' quality. The results are shown in section 1.4. All in all, 79 modules went through the QC procedure – 43 diamond modules and 36 silicon modules, 12 of the latter only for testing purposes. Figure 1.6 shows their production with time. 18 diamond modules and 6 silicon modules were in the end chosen to be made up into DBM telescopes and installed into ATLAS.

A very important issue was the so called erratic current. This term describes the leakage current in a pCVD diamond that becomes unstable. It can develop gradually or can be triggered with a β source. Spikes appear in the otherwise stable leakage current. They can be up to three orders of magnitude higher than the base current. Sometimes the current also suddenly increases for a few orders of magnitude and stays at that level (e.g. from the initial 1 nA to 3 μA). The amplitude differs in magnitude from sensor to sensor. This effect is still not fully explained, but the hypothesis is that the charges find a conductive channel along the grain boundaries, causing discharges. These discharges are picked up by the pixel amplifiers in the FE-I4. A single discharge can trigger a group of up to \sim 500 pixels, resulting in a *blob* on the detector occupancy map. Sometimes the conductive channel stays in a conductive state, making one or more pixels always to fire. These pixels are useless and have to be masked out during measurements.

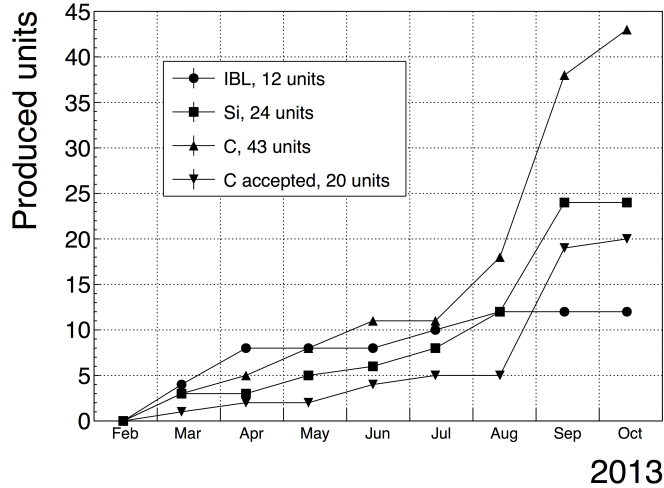


Figure 1.6: Module production with time

231 1.3.3 Installation and commissioning

232 The DBM modules that passed the QC tests were assembled into telescopes – sets of
 233 three modules one behind the other with a spacing of 50 mm. Of the 18 diamond and
 234 6 silicon modules, 6 diamond and 2 silicon modules were built. A special care was
 235 taken when choosing the sets of three diamonds. The modules with a similar pseudo-
 236 efficiency, leakage current, maximum stable high voltage and shape of disconnected
 237 regions were grouped together. After assembly into telescopes, the modules were
 238 tested for their connectivity. Then the high voltage was applied and the leakage
 239 current was observed. This was an important point to check because all three modules
 240 shared the same high voltage channel. Any instabilities on one of the modules would
 241 cause problems on the other two. This would for instance happen if one of the modules
 242 had a much lower breakdown voltage.

243 Due to time constraints, the telescopes were not built at the same time but in-
 244 stead in a pipeline. As soon as two telescopes were ready, they were transported
 245 to Point 1 – the ATLAS site. There they were prepared for installation onto the
 246 pixel detector structure that had been extracted from ATLAS due to pixel detec-
 247 tor commissioning. The commissioning was nearing the end, so the technicians were
 248 preparing the detector for re-insertion. The cylindrical structure was being closed
 249 off by four new service quarter-panels (nSQPs). This meant that with every day the
 250 access to the place of installation of the DBM was more difficult to reach. The first
 251 two telescopes were put into place when only one nSQP was in place. This allowed
 252 the process to be conducted from both sides. This proved to be helpful, because the
 253 process was lengthy and had to be done with great precision. It involved tightening
 254 of several screws on both sides of the telescopes. At the same time the surrounding
 255 electronics and cables had to be left untouched. The lessons learnt with the first part
 256 of the installation were helpful when installing the other telescopes. The last two
 257 were fitted onto the structure when three nSQPs were already in place, leaving only

a narrow opening for access. The whole procedure was carried out blind. After every installation, the telescopes were tested again. First, the low voltage connectivity was checked and a set of tests was run on the FE-I4 front-end chips. An eye diagram was made to estimate the quality of the signal transmission. Then a ^{90}Sr source was used to perform a source test on three modules at the same time. Leakage current was observed during the source test. The final test included running four telescopes (all on one side) at a time. All the tests were successful and the DBM was signed off.

1.4 Performance results

This section gives an overview of the performance results of the DBM modules achieved during the QC and the test beam campaign. The source tests were performed to check for disconnected regions in the sensors and to measure the diamond's pseudo-efficiency. Only the modules with minimal disconnected regions and maximum pseudo-efficiency were chosen for installation.

1.4.1 Source tests

All modules went through the same procedure when tested using a ^{90}Sr source – to check for disconnected regions and to measure the pseudo-efficiency.

The setup consisted of a placeholder for the ^{90}Sr source, an X-Y moving stage with a holder for the module and a scintillator with a photomultiplier placed below the source and the module. The scintillator was used as a trigger – when it detected a particle, it triggered the readout of the module. If the module was placed in between the source and the scintillator, the particle had to traverse the module to hit the scintillator. Therefore, in the case of a module with a 100 % efficiency the triggered data read out by the module would need to contain at least one hit in the module. In reality the β particles scatter around the setup and sometimes hit the scintillator from other directions, without impinging the module. This is the limitation of measuring with a radioactive source as compared to the measurements in a test beam, in which the particles in principle always travel in one direction and their scattering is minimal.

The test for disconnected regions was carried out by moving the module under the source in X and Y direction so that the exposure over the whole plane was uniform. This resulted in an occupancy scan seen in figures 1.7a and 1.7b. The silicon module had a very uniform occupancy plot. So much so that the features of the overlaying flexible PCB can be observed. The rectangular shadows are the passive components whereas the lines are the traces in the PCB. Furthermore, a circular-shaped edge of the PCB can be seen on the bottom right side of the plot. These darker areas are such because fewer electrons can penetrate the material with a high density. In the case of the diamond, the features of the PCB can be observed as well, but are much less distinguishable. In principle, the plot is much more granulated – less uniform. This high variance in the diamond's detection ability is due to the grain boundaries

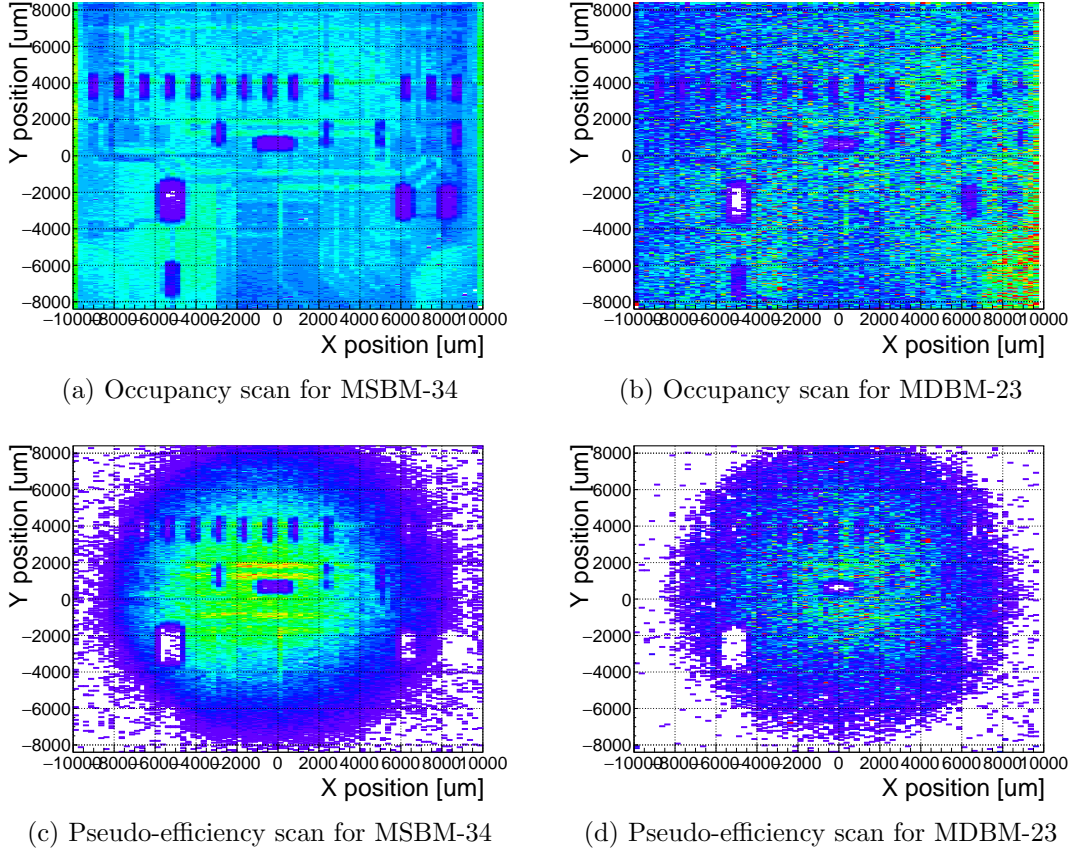
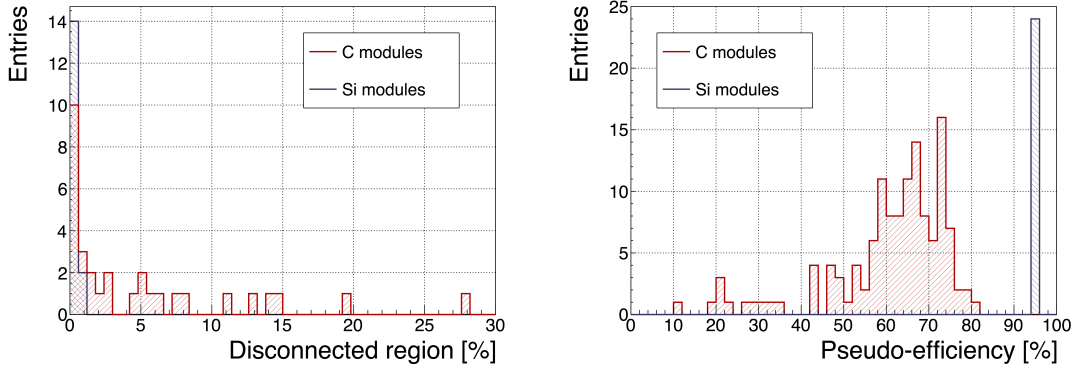


Figure 1.7: Occupancy and pseudo-efficiency scans for the silicon (left) and diamond sensor (right) to check for disconnected regions and estimate the sensor’s efficiency. Shadows of the electronic components are clearly visible because fewer electrons were able to traverse through such a higher amount of material.

in the pCVD material which trap the drifting charges, rendering some regions much less efficient.

The pseudo-efficiency test was carried out by placing the module directly below the source and collimating the particles so that their trajectory was impinging the module in the middle. For every trigger by the scintillator, a script checked whether there was a hit recorded in the module or not. The resulting ratio between the number of triggers and number of hits recorded in the module is a pseudo-efficiency – an estimation of the sensor’s efficiency. It cannot give a precise value due to the triggers produced by scattered particles, but at least gives a rough estimate.

Figure 1.8a shows the distribution of disconnected regions across all tested modules. Silicon modules were performing as expected, with a minimum number of disconnected pixels. The majority of the silicon modules yielded the pseudo-efficiency of $(94.3 \pm 0.2)\%$. Silicon sensors being 99.99 % efficient, this value was underestimated by about 5 %. The measured pseudo-efficiency of the diamond modules was $(65 \pm 7)\%$, with outliers down to 10 %. The value depended on the diamond quality,



(a) Disconnected regions for all modules derived from the occupancy scans

(b) Pseudo-efficiencies for all modules at various threshold and voltage settings

Figure 1.8: Measurements of pseudo-efficiency and disconnected regions for all modules that went through the QC procedure

311 the set threshold and the applied bias voltage. The latter two settings were varied to
 312 check the behaviour of the modules under various conditions.

313 1.4.2 Test beam results

314 The first two assembled prototype DBM modules, MDBM-01 and MDBM-03, were
 315 tested at DESY, Hamburg, in a test beam facility. The aim of the measurements was
 316 to measure their efficiency, the spatial distribution of the efficiency and the effect of
 317 the beam on the disconnected regions. A silicon module MSBM-02 was measured
 318 to crosscheck the measurements. Since the silicon module is almost 100 % efficient,
 319 it was used as an "anchor" – the diamond's efficiency was measured relative to the
 320 silicon's efficiency. Two beam telescopes were used as reference systems: Kartel [],
 321 built by JSI institute from Ljubljana, and EUDET Aconite []. Both are instrumented
 322 with six Mimosa26 pixel planes and capable of tracking particles with a 2 μm tracking
 323 resolution.

324 The test beam prototypes did not meet the acceptance criteria for production
 325 DBM modules in the following areas: first, the CCDs were slightly below 200 μm ,
 326 which would be the DBM minimum. Secondly, the applied bias voltages ranged
 327 from 1–2 V/ μm . In addition, the threshold cut could only be set to 1500 electrons,
 328 which is higher than the DBM minimum (1000 e). Nonetheless, the resulting module
 329 efficiencies were still in the range between 75–85 %.

330 To analyse the test beam data, Judith [] software framework was used. Judith is
 331 capable of synchronising data streams from several detector systems only connected
 332 via a trigger system, reconstructing tracks and calculating efficiency for the DUTs. It
 333 was also used to reconstruct and analyse the acquired Kartel test beam data together
 334 with the silicon and diamond module as DUTs. A sample of the analysed data is shown
 335 in figure ??.



Figure 1.9: This photo highlights four telescopes installed onto the nSQPs and around the pipe

³³⁶ **1.5 Operation**

³³⁷ **1.5.1 Positioning**

³³⁸ The DBM is placed in the forward region of the ATLAS detector, very close to the
³³⁹ beam pipe (see figure 1.9). The mechanical structure that holds the sensor planes is,
³⁴⁰ due to its shape, referred to as a DBM telescope. A telescope is a system that consists
³⁴¹ of several pixel sensors placed in series one behind the other. Each DBM telescope
³⁴² houses three diamond pixel modules. Eight DBM telescopes reside approximately
³⁴³ 1 m away from the collision region, four on each side. They are tilted with respect
³⁴⁴ to the beam pipe for 10°. This is due to a specific phenomenon connected to erratic
³⁴⁵ (dark) currents in diamond. Studies have shown [] that the erratic leakage currents
³⁴⁶ that gradually develop in diamond can be suppressed under certain conditions. For
³⁴⁷ instance, if a strong magnetic field is applied perpendicular to the electric field lines
³⁴⁸ in the diamond bulk, the leakage current stabilises []. The DBM was designed to
³⁴⁹ exploit this phenomenon. The magnetic field lines in the ATLAS experiment are
³⁵⁰ parallel to the beam. Hence, an angular displacement of the sensor with respect to
³⁵¹ the beam allows for the leakage current suppression. However, the DBM telescopes
³⁵² still need to be directed towards the interaction region. Taking these considerations
³⁵³ into account, a 10° angle with respect to the beam pipe was chosen. The influence

Figure 1.10: Occupancy of individual modules during collisions. Only 16 modules were taking data.

354 of the magnetic field on the particle tracks at this angle is very low as the field lines
355 are almost parallel to the tracks. The tracks are therefore straight, which reduces the
356 track reconstruction complexity.

357 1.5.2 Data taking during collisions

358 The DBM has been commissioned in ATLAS and is now taking data. Several issues
359 still need to be resolved regarding the readout systems. Unfortunately, due to issues
360 with the low voltage power supply regulators, six out of 24 modules were damaged
361 during operation: four silicon and two diamond modules. The system configured
362 the modules into an unsteady state whereby they drew twice as much current as the
363 allowed maximum. This current most probably fused the wire bonds within minutes.
364 This has left only five diamond telescopes fully operational. The preliminary data
365 obtained using the remaining telescopes show that the background rejection could
366 indeed work.

367 The first step of the system test was to take data during collisions and check
368 the occupancy in the individual modules. The occupancies were plotted side by side
369 for comparison. Figure 1.10 shows some of the occupancy values. At the time, the
370 readout system was not yet configured to read out all telescopes in parallel.

371 The second step was to test the detector’s capability of particle tracking. Only one
372 telescope was used to take data with the beam. If all three planes of the telescope
373 were hit during a bunch crossing, a linear line was fitted to the hits. This line
374 represented the particle’s trajectory. It was projected towards the interaction point.
375 Two parameters were calculated where the line is the closest to the interaction point:
376 the radial distance and the longitudinal distance between the line and the interaction
377 point (see figure 1.11). This was done for the events with two colliding bunches as
378 well as for events with only one, non-colliding bunch. In principle the tracks recorded
379 during the events with two colliding bunches could either come from the collisions or
380 could be background scattering. Tracks recorded during a non-colliding bunch, on
381 the other hand, are definitely background particles since, in principle, there should
382 be no collisions taking place.

383 A comparison of the data acquired (see figure ??) showed that, for the colliding
384 bunches, the majority of the reconstructed tracks had the origin in the interaction
385 point, with an expected spread in Z and R . For non-colliding bunches, the distribu-
386 tion is more spread out. In the Z_0 distribution it has one peak in the middle, which
387 means that the empty RF buckets still held some particles. The two peaks on the
388 sides, however, show that a significant number of tracks had their origin at the beam
389 pipe. Therefore these tracks were made by stray protons colliding with the beam
390 pipe. These collisions are unwanted as they do not produce any meaningful physics

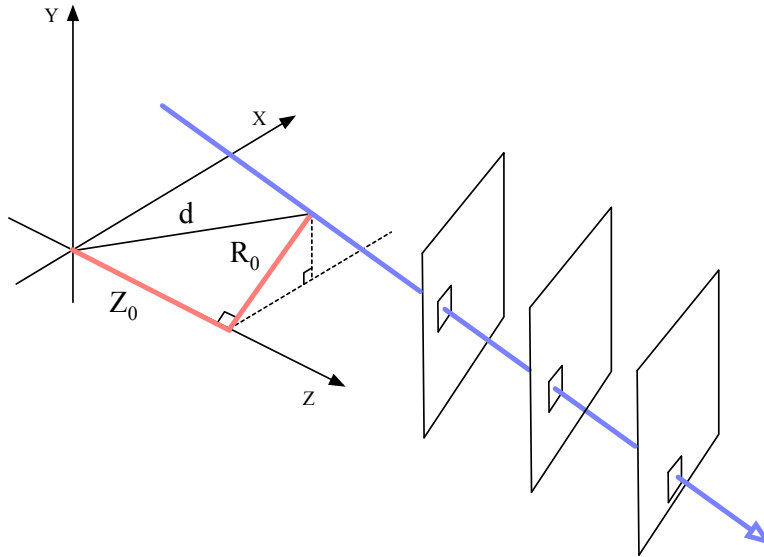


Figure 1.11: A diagram showing the radial distance R_0 and longitudinal distance Z_0 of the trajectory from the interaction point at the minimal distance d . Z is the axis along the beam line. Three module planes intercept a particle and reconstruct its trajectory.

Figure 1.12: These plots show two parameters of particle tracks recorded by one of the DBM telescopes: radial and longitudinal distance of the projected tracks from the interaction point.

³⁹¹ while still damaging the ATLAS detector by means of the produced radiation.

³⁹² 1.6 Conclusion

³⁹³ The Diamond Beam Monitor has been designed as an upgrade to the existing lu-
³⁹⁴ minosity detectors in the ATLAS experiment. It is the first diamond pixel tracking
³⁹⁵ detector installed in a high-energy physics experiment. The pixelated front-end elec-
³⁹⁶ tronic chips ensure precise spatial detection of the charged high-energy particles. The
³⁹⁷ projective geometry allows for particle tracking and background rejection. The de-
³⁹⁸ tector is placed in a high-radiation forward region of the experiment. Therefore,
³⁹⁹ radiation hardness of the chosen pCVD diamond sensors is an important require-
⁴⁰⁰ ment. The tests carried out in the test beam and in the laboratory confirmed that
⁴⁰¹ the DBM modules were ready to be installed in the experiment. The DBM is now
⁴⁰² running in ATLAS during collisions. Further improvements have to be made on the
⁴⁰³ readout firmware before it is included in the main readout stream.